M. CAN ŞENEL[1]*, M. GÜRBÜZ[1]

INVESTIGATION ON MECHANICAL PROPERTIES AND MICROSTRUCTURES OF ALUMINUM HYBRID COMPOSITES REINFORCED WITH Al$_2$O$_3$/GNPs BINARY PARTICLES

Nowadays, aluminum-based composites have been produced by pure alumina (Al$_2$O$_3$) or pure graphene nanoplatelets (GNPs) in aluminum matrix because of the high compressive strength of alumina and the solid lubricant properties of graphene. However, there are no studies on the influence of both alumina and graphene reinforced aluminum composites. In this study, Al-Al$_2$O$_3$ and Al-Al$_2$O$_3$-GNPs composites were reinforced with pure alumina (between 0 and 30 wt.%), pure graphene (0, 0.1, 0.3, 0.5 wt.%), and their hybrid forms (Al$_2$O$_3$-GNPs) by the powder metallurgy method. This method involved ultrasonic dispensing, mixing, filtering, drying, pressing, and sintering processes. From the test results, the micro Vickers hardness of pure aluminum (28.2±1 HV) improved to 51.5±0.8 HV (Al-30Al$_2$O$_3$) and 63.1±1 HV (Al-30Al$_2$O$_3$-0.1GNPs). Similarly, the ultimate compressive strength (UCS) enhanced from 92.4±4 MPa (pure aluminum) to 165±4.5 MPa (Al-30Al$_2$O$_3$) and 188±5 MPa (Al-30Al$_2$O$_3$-0.1GNPs), respectively. In conclusion, the Vickers hardness and ultimate compressive strength of aluminum hybrid composites improved up to 0.1 wt.% graphene content. After 0.1 wt.% graphene content, these mechanical properties decreased because of the clumping of graphene nanoparticles.
Keywords: composite, aluminum, graphene, alumina, hybrid

1. Introduction

Metal matrix composites (MMCs) are reinforced with a carbon-based or a ceramic material into a metal matrix material to enhance its wear and corrosion resistance, strength, and modulus of elasticity [1,2]. MMCs combine the metallic properties of the matrix (high ductility and toughness, etc.) with ceramic and carbon-based properties of reinforcements (high hardness, high strength, etc.) [3]. In MMCs, the most preferred matrix materials are aluminum (Al), magnesium (Mg) and its alloys. Also, metal oxides (Al$_2$O$_3$, ZrO$_2$, SiO$_2$, etc.), metal carbides (B$_4$C, SiC, WC etc.), metal nitrides (TiN, Si$_3$N$_4$, TaN, ZrN etc.), and carbon-based materials (carbon nanotube (CNT), graphene nanoplatelets (GNPs)) can be used as the reinforcement element [4]. Nowadays, the use of pure ceramic (Al$_2$O$_3$, SiC, Si$_3$N$_4$, etc.) or pure carbon-based material (CNT, GNPs, etc.) as the reinforcement element does not meet the desired mechanical properties for aluminum-matrix composites. For this reason, aluminum hybrid composites (Al-Al$_2$O$_3$-GNPs) were developed in order to have superior mechanical properties [5-7].

In general, the melting, squeeze casting, and powder metallurgy (PM) are used to fabricate the MMCs [8]. Among these methods, the PM method is remarkable because of its ability to fabricating complex and self-lubricating machine parts [9-11]. One of the most commonly preferred metals is aluminum for producing the composite materials by the PM method. Aluminum and its alloys are widely employed in automotive, aviation, space and transportation applications due to their good strength, excellent corrosion resistant, and lightweight [12,13]. Also, aluminum and its alloys are easy to recycle from scrap thereby decreasing the greenhouse gas emissions. Among carbon-based reinforcement elements, graphene nanoplatelets have a single layer of graphite, high surface area, and two-dimensional with covalently bonded structure [14-18]. Graphene is one of the most preferred reinforcement material for MMCs due to high mechanical [19], electrical [20], thermal [4], and tribological properties [21-23]. The tensile strength, elasticity modulus, and thermal conductivity of graphene are nearly detected as 130 GPa, 1.0 TPa, and 5000 Wm^{-1}K^{-1}, respectively [24]. The other preferred reinforcement element for MMcs is expressed as alumina (Al$_2$O$_3$) which has a high compressive strength, high hardness, and good wear resistance.

In the current literature, most papers were focused on the mechanical properties of Al-Al$_2$O$_3$ [3,13,25,26] and Al-GNPs [27-34] composites. Kok [3] investigated the mechanical properties of alumina reinforced aluminum composites with different particle

[1] ONDOKUZ MAYIS UNIVERSITY, MECHANICAL ENGINEERING DEPARTMENT, SAMSUN, TURKEY

* Corresponding author: mahmutcan.senel@omu.edu.tr
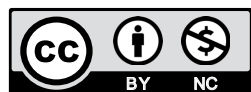
sizes (Al$_2$O$_3$: 66, 16, 32 μm) and weight percentages (Al$_2$O$_3$: 10, 20, 30 wt.%). The results showed that the tensile strength and the hardness of the composites improved with a reduction in the particle size and a rise in the reinforcement ratio of particles. Srivastava and Chaudhari [13] studied the mechanical properties and microstructure of Al6061-nano alumina composites with various weight percentages (1, 2, 3 wt.%). Vickers hardness (~76%) and yield strength (~81%) of Al6061-2%Al$_2$O$_3$ composite were improved compared to those of Al6061 alloy. After 2% nano Al$_2$O$_3$ content, the mechanical properties of composites decreased due to the formation of microcracks. Ezatpour et al. [25] examined the effects of nano Al$_2$O$_3$ content (0.4, 0.8, 1.2 wt.%) on the mechanical properties and microstructures of Al7075-nano alumina composite. The best strength was obtained at Al-0.4%Al$_2$O$_3$ composite. After this nano Al$_2$O$_3$ content, the mechanical properties of composites were deteriorated due to the agglomeration of nano Al$_2$O$_3$ particles. Bastwros et al. [27] examined the strength of Al-GNPs composites. Improvement in strength (~47%) was detected compared to aluminum alloy (Al6061). Rashad et al. [28] researched the mechanical properties and microstructures of graphene-reinforced Al composites. The tensile strength and the yield strength of Al-0.3%graphene were improved the rate of ~11.1% and ~14.7%, respectively. On the other hand, the compressive strength was decreased the rate of ~7.8% when compared to pure aluminum. Li and Xiong [29] focused on the microstructure and the tensile properties of Al-GNPs composites with different weight percentages (GNPs: 0.25, 0.5, 1 wt.%). The enhancement in yield strength and tensile strength of Al-GNPs composite was determined as ~38.27% and ~56.19%, respectively compared to pure aluminum. Gürbüz et al. [30] examined the influence of sintering conditions and GNPs amount on the density, microstructure, and Vickers hardness of graphene-reinforced aluminum composites. The optimum GNPs amount, sintering temperature, and sintering time were determined as 0.1 wt.%,

630ºC, and 180 min, respectively. According to the literature survey, there has been no publication related to the mechanical and microstructural properties of Al-Al$_2$O$_3$-GNPs hybrid composites. For this reason, new generation aluminum composites (Al-GNPs etc.) and their hybrid forms (Al-Al$_2$O$_3$-GNPs etc.) should be developed as a new class of superior engineering material.

In this study, Al-Al$_2$O$_3$ and Al-Al$_2$O$_3$-GNPs composites with various Al$_2$O$_3$ and GNPs content were fabricated by powder metallurgy method. This works aims to examine the influence of Al$_2$O$_3$ and Al$_2$O$_3$-GNPs amount on the hardness, apparent density, microstructure, and compressive strength of Al matrix composites.

2. Experimental procedures

2.1. Materials

In the present work, atomized pure aluminum powders (the purity of 99%, the particle diameter of 8-15 μm, and the theoretical density of 2.7 g/cm^3) were used as the matrix material while alumina and graphene powders were used as the reinforcement material. Aluminum and alumina powders were provided by Alfa Aesar Inc. (United Kingdom) and Hindalco Ind. (India), respectively. The particle size and theoretical density of alumina powders were nearly ~4 μm and 3.97 g/cm^3, respectively. Graphene nanoplatelets (the typical surface area of 120-150 m^2/g, the theoretical density of 2.25 g/cm^3, and the thickness of 5-8 nm) were supplied by Grafen Chemical Ind. Co. (Turkey).

2.2. Fabrication of composite materials

Fig. 1 demonstrates the fabrication scheme of graphene-alumina reinforced aluminum hybrid composites by powder
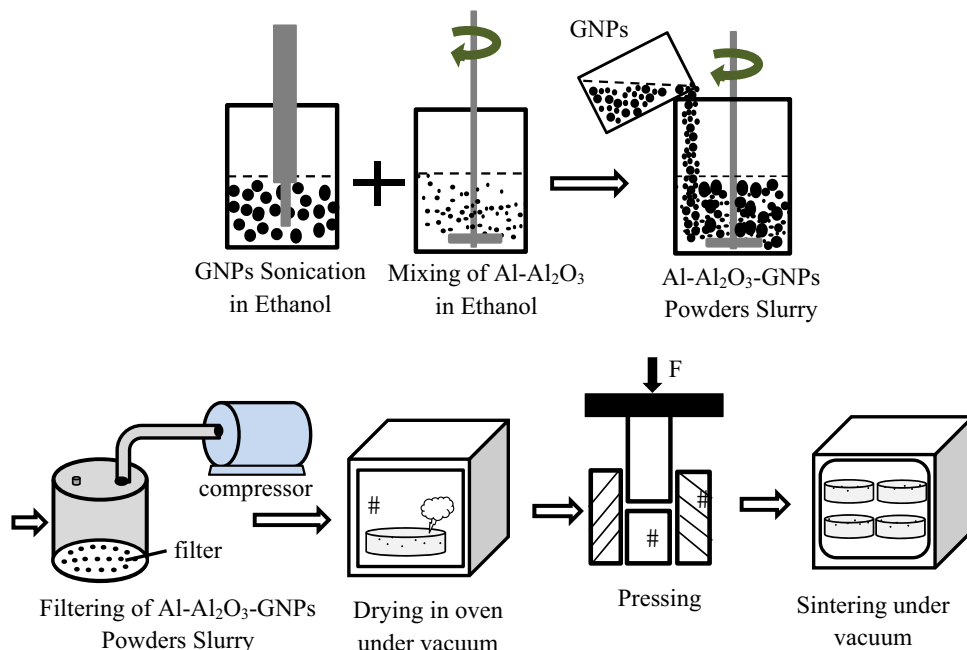

Fig. 1. The fabrication scheme of Al-Al$_2$O$_3$-GNPs hybrid composites by PM method

metallurgy method. Aluminum and alumina (1, 3, 6, 9, 12, 15, 18, 21, 25, 30 wt.%) powders were mixed in ethanol using the mechanical mixer. At the same time, graphene nanoparticles (0.1, 0.3, 0.5 wt.%) were blended in ethanol by using ultrasonic dispenser. Then, the graphene solution was added to the aluminum-alumina solution. The prepared solution was filtered and dried at 45°C for overnight. The powders were compacted in a stainless steel die under a pressure of 650 MPa. Then, the samples were sintered in a tube furnace under vacuum. The sintering time (t_S = 180 min) and the sintering temperature (T_S = 630°C) were detected as our previous study [30]. A similar process was performed for the fabrication of pure alumina reinforced Al matrix composites.

2.3. Characterization

The microstructure of powders and composites were investigated by using scanning electron microscope (SEM, Jeol JSM-7001F). In order to detect the distribution of alumina and graphene in the Al matrix, line scan and Energy Dispersive X-Ray (EDX) map analyses were carried out by SEM. In order to determine the distribution of alumina and graphene in the Al matrix, X-ray Diffraction (XRD, Rigaku Smartlab) analysis was used to examine the phases in composites and powders. Raman spectroscopy (Renishaw inVia) for 532 nm wavelength was used to detect the presence of GNPs in the aluminum hybrid composite. The particle size distribution of the powders was detected by Malvern Mastersizer 3000 particle size analyzer.

The apparent densities of samples were obtained by Archimedes principle. The density results were averaged over at least six measurements. The Vickers hardness of the composites was measured by the HV-1000B micro Vickers hardness tester under 200 g load with the dwell time of 15 s. To prevent the segregation effects, the mean of six measurements from polished cross-sections was taken for each specimen. The compressive strength of the composites was determined by the compressive test unit (Mares Test-10 tons). In this unit, each composition was tested at least five times with the compression rate of 10 mm/min.

3. Results and discussion

3.1. Characterization of powders

SEM images of pure Al, GNPs, and Al_2O_3, powders are presented in Fig. 2. The morphology of aluminum and alumina powders has an irregular form (Fig. 2(a) and (b)). Graphene nano-
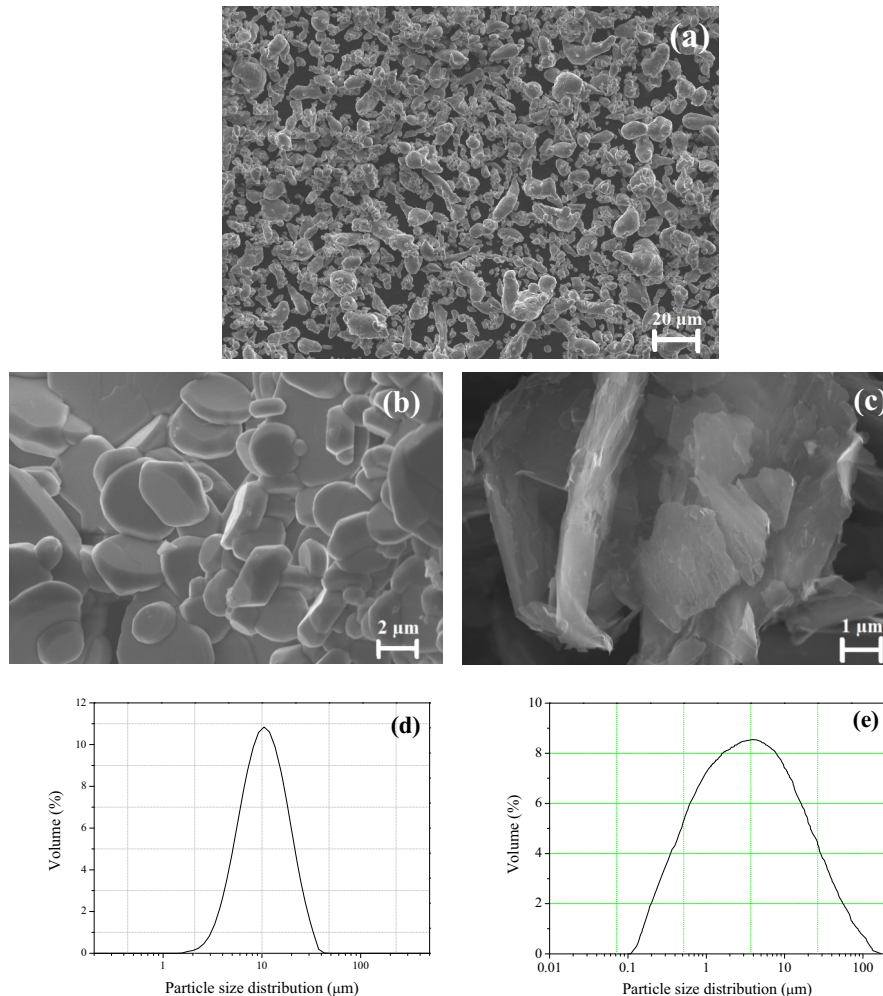

Fig. 2. SEM images of pure Al (a), alumina (b), and GNPs (c) and particle size distribution of Al (c) and Al_2O_3 (d)

particles have the morphology of two-dimensional and plate-like as given in Fig. 2(c). The mean particle sizes of aluminum and alumina powders are determined as ~10 µm and ~4 µm (Fig. 2(d) and (e)). These analyses confirmed by the SEM image analyses.

Fig. 3(a)-(c) gives the XRD plots of pure Al, Al_2O_3, and GNPs, respectively. As seen from these figures, GNPs, aluminum, and Al_2O_3 peaks are presented at $2\theta = \sim26.5°$; $2\theta = \sim39°$, $45°$, $65°$, 78; $2\theta = \sim25°$, $35°$, $38°$, $43°$, $53°$, $58°$, $61°$, $67°$, $68°$, $77°$, respectively. The phase analyses of pure powders are a remarkable process to detect the phases of composites after sintering. In addition, these analyses give the information related to the reaction between the matrix and reinforcement elements after sintering.

SEM-EDX elemental distribution of Al, graphene, and alumina in Al-30Al_2O_3-0.1GNPs mixed powders after ultrasonication were presented in Fig. 4. In the figure, C and O distributions imply the graphene and alumina distribution in the aluminum matrix, respectively. As seen from the figure, graphene and alumina were homogeneously distributed in Al-30Al_2O_3-0.1GNPs mixed powders. This analysis is an important process to determine the agglomeration of GNPs in Al-30Al_2O_3-0.1%GNPs composite.

3.2. Mechanical properties of composites

Fig. 5 represents the variation in apparent density of Al-Al_2O_3 and Al-Al_2O_3-GNPs composites. The apparent density variation of Al_2O_3 reinforced aluminum composites was given in Fig. 5(a). It was reported that increasing Al_2O_3

content in Al matrix increased the density due to the high theoretical density of Al_2O_3 (3.97 g/cm^3). The maximum apparent density was determined at Al-30Al_2O_3 (2.70 g/cm^3). Because of having the maximum density among all Al-Al_2O_3 composites, 30 wt.%Al_2O_3 composition was preferred to investigate the influence of graphene amount (varies between 0.1 and 0.5 wt.%) on the compressive strength, Vickers hardness, and apparent density. Fig. 5(b) illustrates the influence of graphene amount (GNPs: 0.1, 0.3, 0.5 wt.%) on the apparent density of Al-30Al_2O_3-xGNPs composites. It can be seen that the apparent density of Al-30Al_2O_3-graphene composite reduced from 2.70±0.02 g/cm^3 to 2.64±0.02 g/cm^3 with increasing graphene content. The low theoretical density of GNPs (2.25 g/cm^3) resulted in a decrease in the apparent density of the composites. Also, the apparent densities of all composites (Al-Al_2O_3, Al-Al_2O_3-GNPs) increased due to the sintering effect compared to the green samples.

The variation in micro Vickers hardness of Al-Al_2O_3 and Al-Al_2O_3-GNPs composites is illustrated in Fig. 6. As shown in Fig. 6(a), the Vickers hardness of Al-Al_2O_3 composite improved with the increase in alumina content due to the hard structure of Al_2O_3 particles. The maximum Vickers hardness value (51.5±0.8 HV) was obtained at Al-30Al_2O_3. Fig. 6(b) presents the influence of graphene content (varies between 0.1 to 0.5 wt.%) on the hardness of Al-30Al_2O_3-graphene composites. The highest hardness value was detected as 63.1±1 HV (Al-30Al_2O_3-0.1GNPs). The distribution of graphene in the aluminum matrix is very important on the mechanical behavior of Al-based composite. Hence, the micro Vickers hardness of
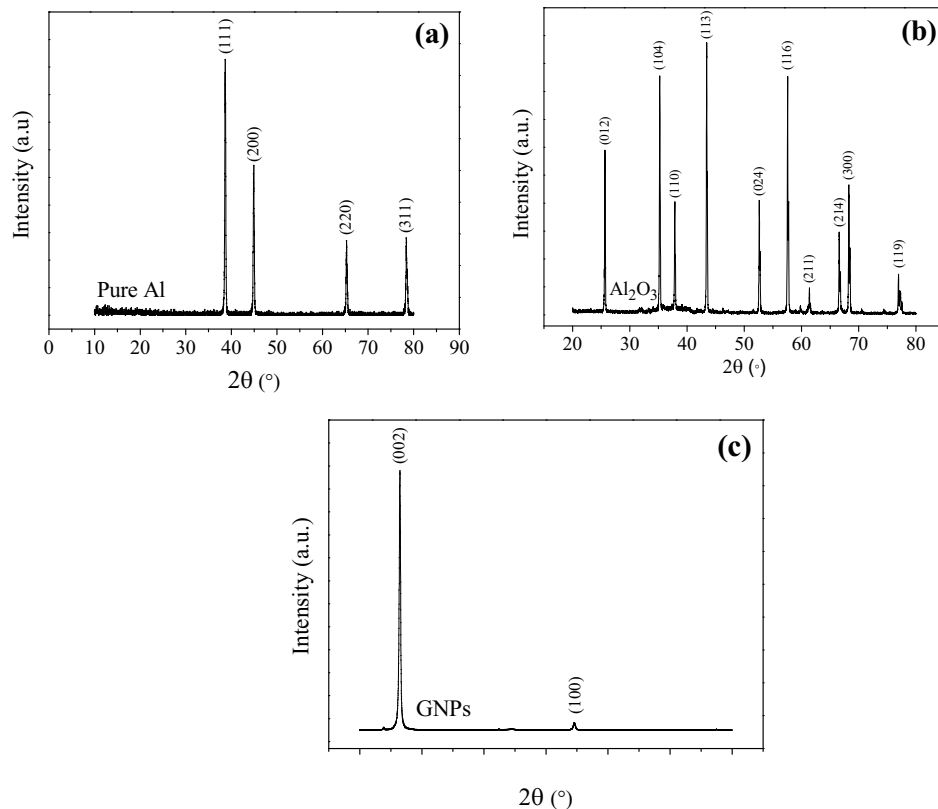

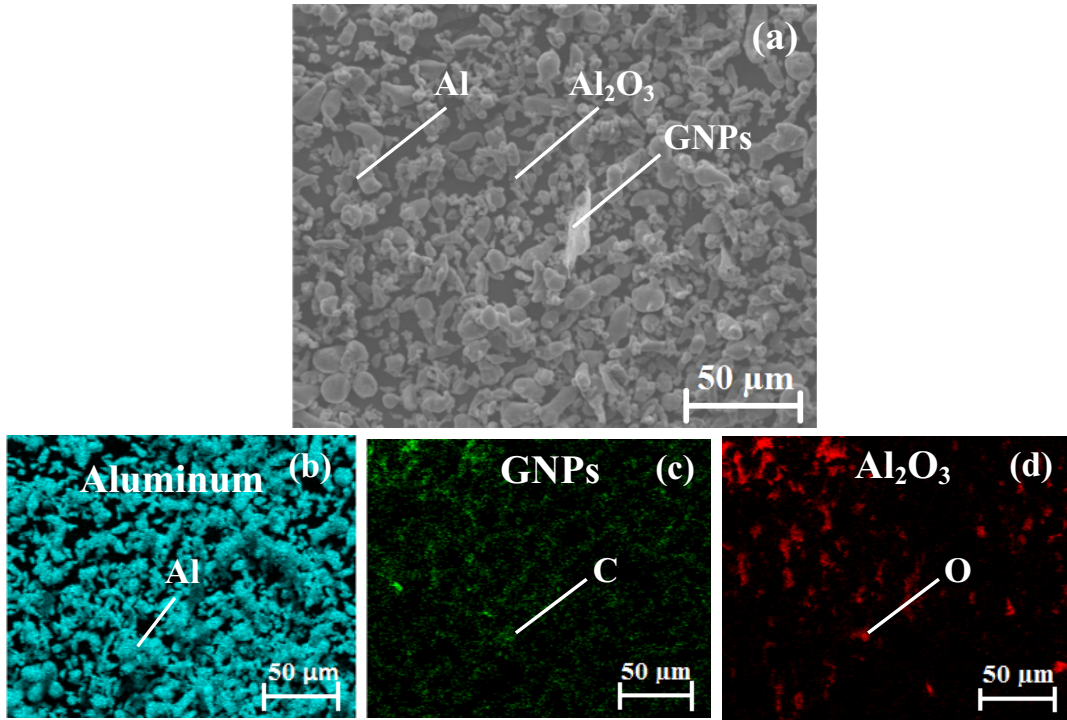Fig. 3. XRD plots of pure Al (a), Al_2O_3 (b), and GNPs (c)

Fig. 4. SEM-EDX elemental distributions of Al (b), graphene (c), and alumina (d) in Al-30Al$_2$O$_3$-0.1GNPs mixed powders (a) after ultrasonication
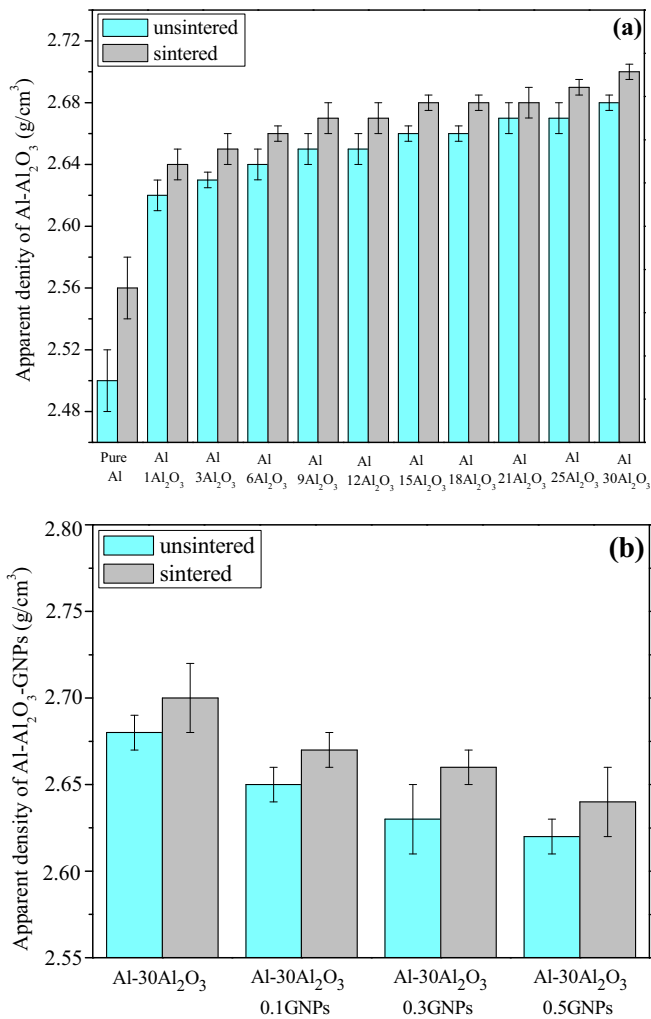

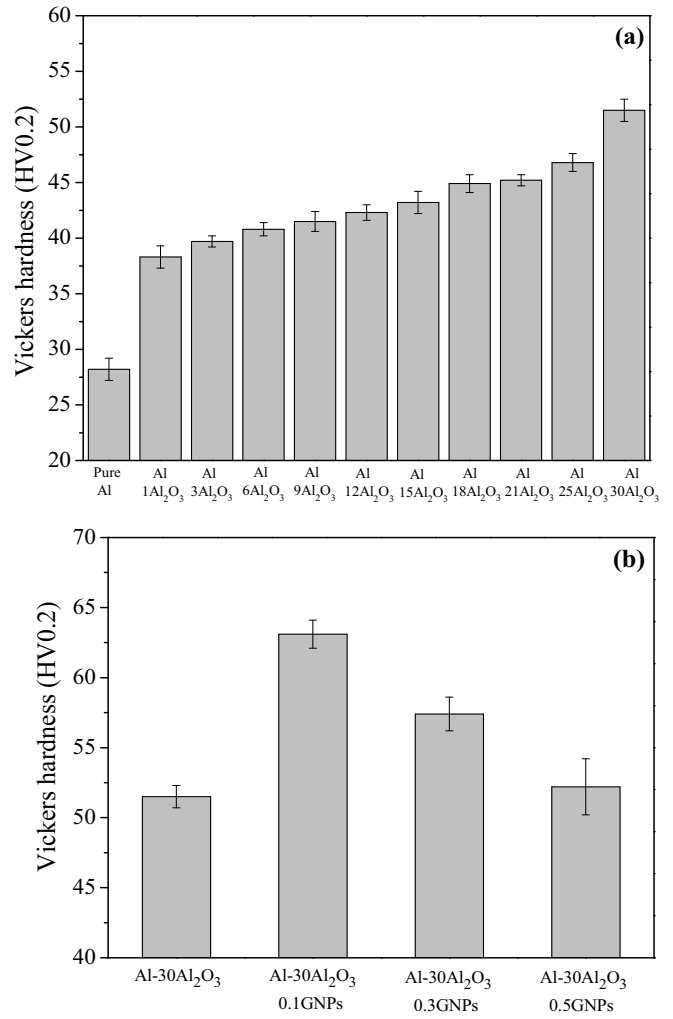Fig. 5. The variation in apparent density of Al-Al$_2$O$_3$ (a) and Al-30Al$_2$O$_3$-xGNPs (b) composites

Fig. 6. The variation in Vickers hardness of Al-Al$_2$O$_3$ (a) and Al-30Al$_2$O$_3$-xGNPs (b) composites

the Al-Al$_2$O$_3$-GNPs composites reduces after 0.1 wt.%GNPs amount due to the clustering of graphene. It is noticed that the interaction between GNPs and aluminum particles decreases with the clustering of graphene during pressing. It leads to more porosity and the worse hardness value [30,35].

The increase in the hardness of the composites can be expressed theoretically with the rule of mixtures by Eq. (1) [36].

$$H_c = H_m f_m + H_r f_r \qquad (1)$$

where f_r and f_m are the volume fraction of reinforcement and matrix element, H_m, H_c, and H_r are the hardness of the matrix, composite, and reinforcement element, respectively.

The increment of the hardness for Al-30Al$_2$O$_3$-xGNPs composite with the addition of GNPs can also be explained by Eq. (2) [35].

$$H = h\sqrt{Dt} + \alpha Gb\sqrt{\rho} \qquad (2)$$

where ρ is the dislocation density, b is Burger's vector, and h, G, α are the constant of the material. The dislocation strengthening controls the hardness of the aluminum hybrid composites which is known as the dislocation density mechanisms. Graphene improved the dislocation density in aluminum composites because of its nano-sized structure. In this work, graphene led to

improving the dislocation density and it caused the increase in the hardness of aluminum hybrid composites.

Fig. 7 gives the variation in ultimate compressive strength (UCS) of Al-Al$_2$O$_3$ and Al-Al$_2$O$_3$-GNPs composites. The UCS of Al$_2$O$_3$ reinforced aluminum composites improved from 92±4 MPa to 165±4.5 (Al-30Al$_2$O$_3$), respectively (Fig. 7(a)). Among Al-Al$_2$O$_3$-GNPs composites, the highest UCS was obtained as 188±5 MPa (Al-30Al$_2$O$_3$-0.1GNPs). The increase in GNPs content up to 0.1%GNPs raised the UCS of Al-Al$_2$O$_3$-GNPs (Fig. 7(b)). Above 0.1%graphene amount, the compressive strength, Vickers hardness, and apparent density reduced due to the easy sliding during deformation and the agglomeration of GNPs. After 0.1 wt.%GNPs content in Al hybrid composites, the poor interface between Al and GNPs involved because of the clustered GNPs. This caused to more porosity and worse compressive strength. Hall-Petch and fine-grained strengthening mechanisms express the enhancement in the compressive strength of Al hybrid composites. In these mechanisms, graphene nanoparticles act as an obstacle to prevent the grain growth. The dislocations do not easily move because of the fine grain microstructure. It caused the enhancement in the compressive strength of Al hybrid composites [37,38].

The increment of graphene nanoparticles amount causes the decreasing the distance between particles as shown in Eq. (3) [36].

$$\lambda = \left[4(1-f)r \right] / (3f) \qquad (3)$$

In this equation, f is the volume fraction of the graphene, r is the radius the graphene, and λ is the distance between the reinforcement elements. Eq. (4) expresses the relation between shear stress (τ_0) and the distance between the reinforcement particles (λ) [36]:

$$\tau_0 = Gb/\lambda \qquad (4)$$

where G is shear module and τ_0 is shear stress. By evaluating Eq. (3) and (4), the drop in the distance between particles improved the strength of composites [39,40]. Graphene act as an obstacle in the grain boundaries. In addition, it prevents the dislocation movement. By adding GNPs to the Al matrix, the distance between particles reduced and then the movement of the dislocation resisted. For this reason, graphene nanoparticles cause more barriers and dislocations pile-up begins. The strength of the composite can be defined as given in Eq. (5) [36]:

$$\sigma_c = \sigma_m f_m + \sigma_r f_r \qquad (5)$$

where f_r, f_c, and f_m are the volume fraction of reinforcement, composite, and matrix material, σ_r, σ_c, and σ_m are the strength of the reinforcement, composite, and matrix material.

3.3. Characterization of sintered composites

XRD plots of pure Al, Al-30Al$_2$O$_3$, and Al-30Al$_2$O$_3$-xGNPs composites are given in Fig. 8(a). To detect the formation of α-Al$_2$O$_3$ and GNPs in Al composite, XRD analysis was actualized for pure Al, Al-30Al$_2$O$_3$, and Al-30Al$_2$O$_3$-xGNPs composites.
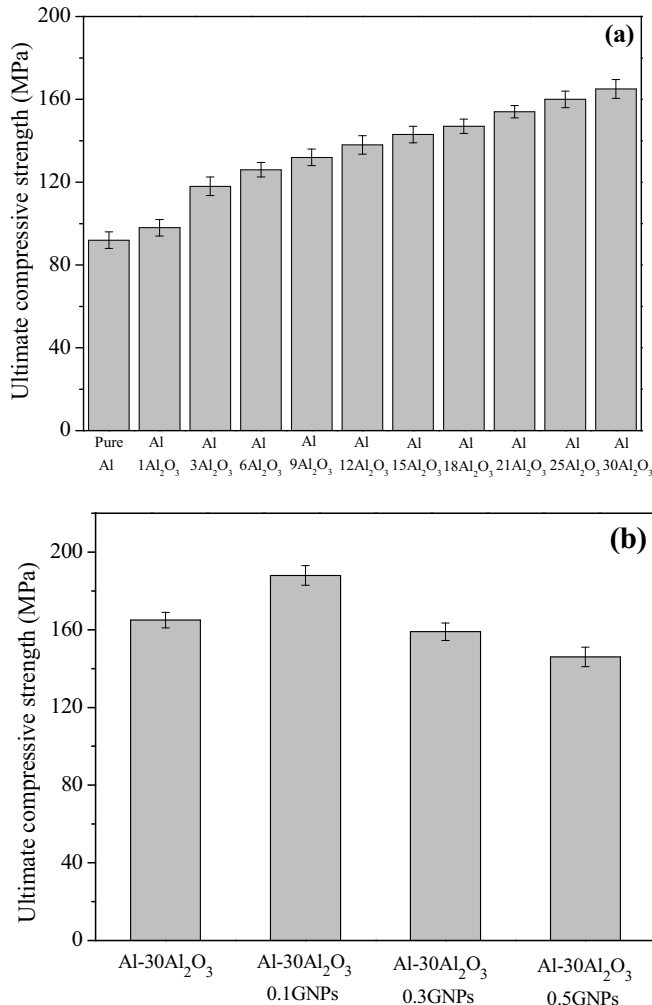

Fig. 7. The variation in UCS of Al-Al$_2$O$_3$ (a) and Al-30Al$_2$O$_3$-xGNPs (b) composites

As seen from the figure, the intensity of α-Al_2O_3 peaks in Al composites increased with increasing Al_2O_3 content. The peak angles (2θ = ~25°, 35°, 38°, 43°, 53°, 58°, 61°, 67°, 68°, 77°) of Al_2O_3 was verified with the existence of α-Al_2O_3 in Al-Al_2O_3 and Al-Al_2O_3-GNPs composites. From the XRD analysis, the undesired phase formation such as Al_4C_3 was not observed in any composition. Also, graphene peak (2θ = 26.5°) was not detected in any aluminum hybrid composite due to the low content of graphene. For this reason, the Raman spectroscopy analysis was performed in order to detect the existence of graphene in Al-$30Al_2O_3$-0.1GNPs composite (Fig. 8(b)). The main band range of carbon materials varies from 1200 to 2800 cm^{-1}. The existence of graphene nanoplatelets was confirmed by the given peaks (D, G, and 2D band at 1342, 1583, and 2680 cm^{-1}, respectively). These results obtained from XRD and Raman analyses are in agreement with the literature [41,42].
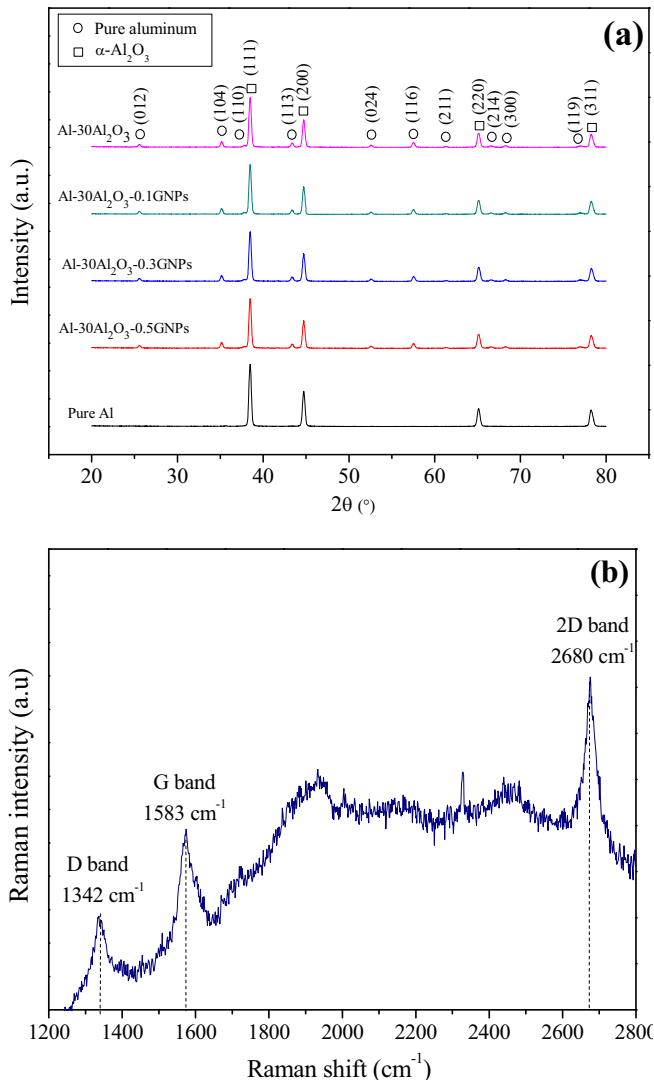
elements were defined as C from GNPs, O from Al_2O_3, and Al. Graphene nanoparticles had the uniform distribution in the Al-$30Al_2O_3$-0.1GNPs composite (Fig. 9(a)). From the SEM-EDX mapping images of Al-$30Al_2O_3$-0.1GNPs composite, the minimum porosity was observed. In addition, it was determined that graphene placed at the Al grain boundary which created a barrier. This condition enhanced the mechanical properties of Al matrix composites. On the other hand, the clustering of GNPs was seen in the microstructure of Al-$30Al_2O_3$-0.3GNPs and Al-$30Al_2O_3$-0.5GNPs composites (Fig. 9(b) and (c)). These agglomerations deteriorated the mechanical properties of aluminum hybrid composites.

Fig. 10 illustrates the SEM images of Al-$30Al_2O_3$ and Al-$30Al_2O_3$-0.1GNPs composites. From the fracture surface analysis of the composite, it was clearly seen that Al_2O_3 particles were distributed homogeneously and positioned at the between aluminum boundaries. In addition, strong neck formation and well bonding were detected in the microstructure analysis of Al-$30Al_2O_3$ (Fig. 10(a)) and Al-$30Al_2O_3$-0.1GNPs (Fig. 10(b)) composites. On the other hand, the best density, hardness, and compressive strength values were obtained at Al-$30Al_2O_3$ and Al-$30Al_2O_3$-0.1GNPs composites. Thus, the microstructure analyses were verified with the compressive strength and hardness measurement of the composites.

Fig. 11 shows the SEM-EDX line scan analysis of Al-$30Al_2O_3$-0.1%GNPs composite. From this analysis, it was detected that graphene was located at the aluminum grain boundaries. The value of carbon signal had the maximum at the Al grain boundaries because of the existence of graphene. Also, the value of the aluminum signal decreased in the graphene region. This means the particles in the microstructure of aluminum-based composite are refined in small grain size without coarsening of the aluminum. It leads to an enhancement in the density and hardness values of the composites.

Fig. 8. XRD plots of pure Al, Al-$30Al_2O_3$, Al-$30Al_2O_3$-xGNPs composites (a) and Raman spectra of Al-$30Al_2O_3$-0.1GNPs (b) composite

SEM and SEM-EDX mapping images of Al-$30Al_2O_3$-0.1GNPs, Al-$30Al_2O_3$-0.3GNPs, Al-$30Al_2O_3$-0.5GNPs composites are given in Fig. 9. As given in the figure, the main

4. Conclusions

In this work, Al-Al_2O_3 and Al-Al_2O_3-GNPs composites with various Al_2O_3 and GNPs content were fabricated by powder metallurgy method. The influences of Al_2O_3 and Al_2O_3-GNPs amount on the Vickers hardness, apparent density, microstructure, and compressive strength of composites were investigated. The results can be summarized as follows:

- From experimental test results, the optimum Al_2O_3 content for the Al matrix was determined as 30%Al_2O_3. By using this content, Al-$30Al_2O_3$-xGNPs hybrid composites were produced. Among Al hybrid composites, the highest apparent density, Vickers hardness, and compressive strength were obtained at Al-$30Al_2O_3$-0.1GNPs which were measured as 2.67±0.01 g/cm^3, 63.1±1 HV, 188±5 MPa, respectively. After 0.1%GNPs amount, the mechanical properties of Al hybrid composites deteriorated because of the agglomeration of GNPs. These agglomerations resulted in the lower mechanical properties.
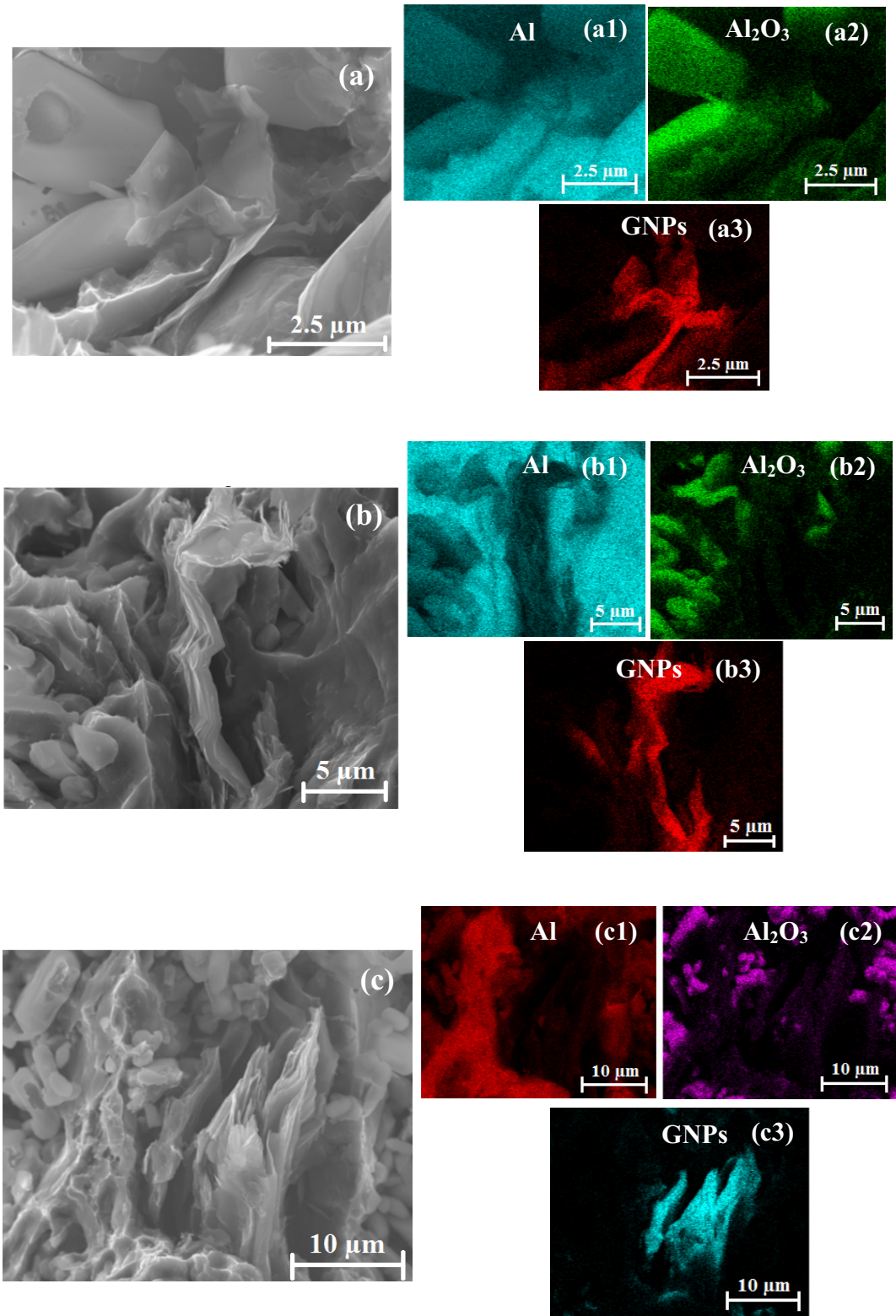
Fig. 9. SEM and SEM-EDX mapping images of Al-30Al$_2$O$_3$-0.1GNPs (a, a1, a2, a3), Al-30Al$_2$O$_3$-0.3GNPs (b, b1, b2, b3), Al-30Al$_2$O$_3$-0.5GNPs (c, c1, c2, c3) composites

- From the SEM analyses, the existence of GNPs and Al$_2$O$_3$ were observed at all aluminum hybrid composites. In all composites, a good neck formation and bonding between the particles were detected. XRD analyses show that peaks of graphene were not seen in any Al-Al$_2$O$_3$-GNPs composites because of the low content of GNPs. Also, an in-situ reaction between aluminum and carbon such as Al$_4$C$_3$ were not detected for all compositions.

- Experimental results showed that GNPs and Al$_2$O$_3$ are well-dispersed into the aluminum matrix. Well-distributed graphene particles act as an obstacle at the grain boundaries. Also, GNPs prevents the grain growth during sintering.
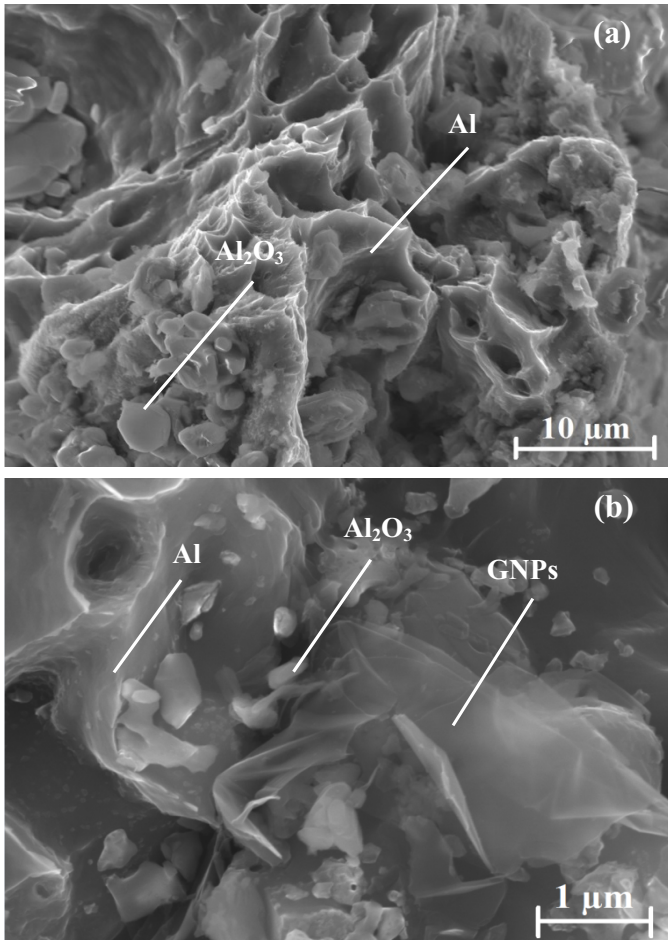
Fig. 10. SEM images of Al-30Al$_2$O$_3$ (a) and Al-30Al$_2$O$_3$-0.1GNPs (b) composites

Fig. 11. SEM-EDX line scan analysis of Al-30Al$_2$O$_3$-0.1GNPs composite

Binary GNPs and Al$_2$O$_3$ create a synergic effect on the mechanical strength of Al-based composites owing to the high compressive strength of ceramic and extraordinary properties of GNPs.

REFERENCES

[1] G.S. Hanumanth,, G.A. Irons, J. Mater. Sci. **28**, 2459-2465 (1993).

[2] Y. Sahin, S. Murphy, J. Mater. Sci. **34**, 5399-5407 (1996).

[3] M. Kok, J. Mater. Process. Tech. **161**, 381-387 (2005).

[4] J.K. Chen, I.S. Huang, Compos. Part B-Eng. **44** (1), 698-703 (2013).

[5] S.J. Yan, S.L. Dai, X.Y. Zhang, C. Yang, Q.H. Hong, J.Z. Chen, Z.M. Lin, Mat. Sci. Eng. A-Struct. **612**, 440-444 (2014).

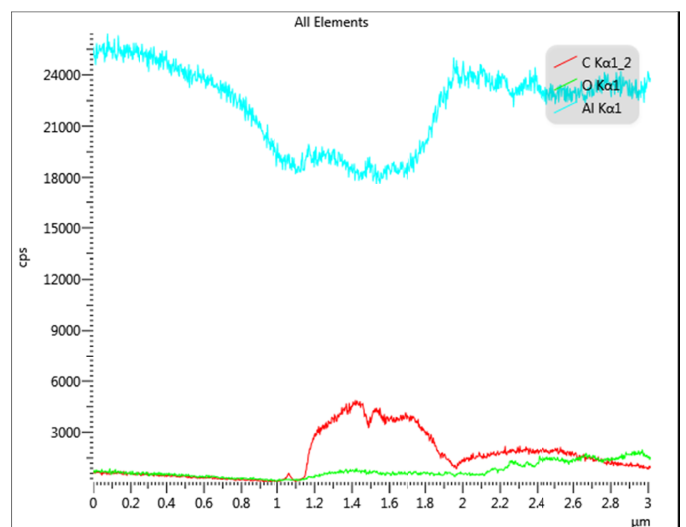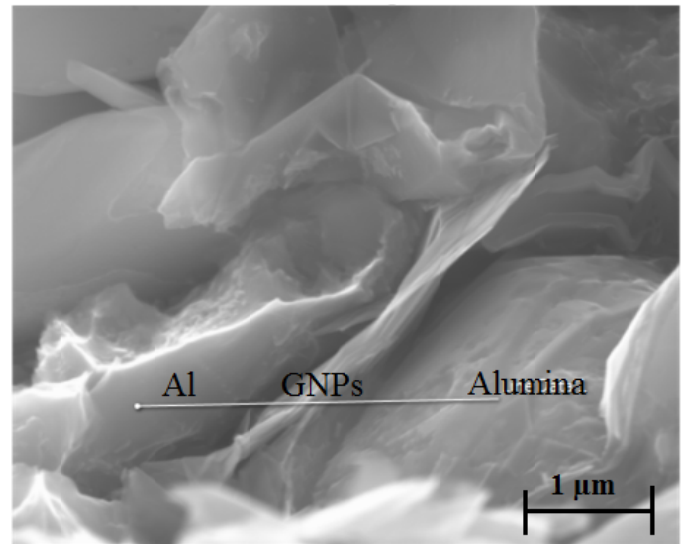[6] F.H. Latief, E.S.M. Sherif, J. Ind. Eng. Chem. **18**, 2129-2134 (2012).

[7] J.L. Li, Y.C. Xiong, X.D. Wang, S.J. Yan, C. Yang, W.W. He, J.Z. Chen, S.Q. Wang, X.Y. Zhang, S.L. Dai, Mat. Sci. Eng. A-Struct. **626**, 400-405 (2015).

[8] A. Saboori, C. Novara, M. Pavese, C. Padini, F. Giorgis, P. Fino, J. Mater. Eng. Perform. **26** (3), 993-999 (2017).

[9] G. O'Donnel, L. Looney, Mat. Sci. Eng. A-Struct. **303**, 292-301 (2001).

[10] O.G. Neikow, S.S. Naboychenko, G. Dawson, Handbook of Non-Ferrous Metal Powders-Technologies and Applications, Elsevier, Amsterdam (2009).

[11] R.S. Rana, R. Purohit, V.K. Soni, S. Das, Mater. Today-Proc. **2** (4-5), 1149-1156 (2015).

[12] M. Zamani, H. Dini, A. Svoboda, L. Lindgren, S. Seifeddine, N. Andersson, A.E.W. Jarfors, Int. J. Mech. Sci. **121**, 164-170 (2017).

[13] N. Srivastava, G.P. Chaudhari, Mat. Sci. Eng. A-Struct. **724**, 199-207 (2018).

[14] J. Wang, Z. Li, G. Fan, H. Pan, Z. Chen, D. Zhang, Scripta Mater. **66** (8), 594-597 (2012).

[15] A.K. Geim, K.S. Novoselov, Nat. Mater. **6**, 183-191 (2007).

[16] E.P. Randviir, D.A.C. Brownson, C.E. Banks, Mater. Today. **17** (9), 426-432 (2014).

[17] N. Savage, Nature. **482**, 30-31 (2012).

[18] V. Singh, D. Joung, L. Zhai, S. Das, S.I. Khondaker, S. Seal, Prog. Mater. Sci. **56** (8), 1178-1271 (2012).

[19] B. Peng, M. Locascio, P. Zapol, S. Li, S.L. Mielke, G.C. Schatz, H.D. Espinosa, Nat. Nanotechnol. **3** (10), 626-631 (2008).

[20] C. Balázsi, B. Fényi, N. Hegman, , F. Wéber, Z. Vértesy, Z. Kónya, I. Kiricsi, L.P. Biró, P. Arató, Compos. Part B-Eng. **37** (6), 418-424 (2006).

[21] M.M.H. Bastwros, A.M.K. Esawi, A. Wifi, Wear. **307** (1-2), 164-173 (2013).

[22] A. Baradeswaran, A.E. Perumal, Compos. Part B-Eng. **56**, 472-476 (2014).

[23] D. Berman, A. Erdemir, A.V. Sumant, Mater. Today. **17** (1), 31-42 (2014).

[24] Y. Zhu, S. Murali, W. Cai, X. Li, J.W. Suk, J.R. Potts, R.S. Ruoff, Adv. Mater. **22** (35), 3906-3924 (2010).

[25] H.R. Ezatpour, M. Torabi Parizi, S.A. Sajjadi, G.R. Ebrahimi, A. Chaichi, Mater. Chem. Phys. **178**, 119-127 (2016).

[26] S.A. Sajjadi, H.R. Ezatpour, H. Beygi, Mat. Sci. Eng. A-Struct. **528**, 8765-8771 (2011).

[27] M. Bastwros, G. Kim, C. Zhu, K. Zhang, S.Wang, X. Tang, X. Wang, Compos. Part B-Eng. **60**, 111-118 (2014).

[28] M. Rashad, F. Pan, A. Tang, M. Asif, Prog. Nat. Sci.-Mater. **24** (2), 101-108 (2014).

[29] G. Li, B. Xiong, J. Alloy Compd. **697**, 31-36 (2017).

[30] M. Gürbüz, M.C. Şenel, E. Koç, J. Compos. Mater. **52** (4), 553-563 (2018).

[31] S.F. Bartolucci, J. Paras, M.A. Rafiee, S. Lee, D. Kapoor, N. Koratkar, Mat. Sci. Eng. A-Struct. **528** (27), 7933-7937 (2011).

[32] M.C. Şenel, M. Gürbüz, E. Koç, J. Mater. Sci. Technol. **34** (16), 1980-1989 (2018).

[33] R. Pérez-Bustamante, D. Bolaños-Morales, J. Bonilla-Martínez, I. Estrada-Guel, R. Martínez-Sánchez, J. Alloy Compd. **615** (1), 578-582 (2014).

[34] M.C. Şenel, M. Gürbüz, E. Koç, Compos. Part B-Eng. **154**, 1-9 (2018).

[35] M. Gürbüz, T. Mutuk, J. Compos. Mater. **52** (4), 543-551 (2018).

[36] G.E. Dieter, Mechanical Metallurgy, McGraw-Hill, New York (1986).

[37] Z. Hu, G. Tong, Q. Nian, R. Xu, M. Saei, F. Chen, C. Chen, M. Zhang, H. Guo, J. Xu, Compos. Part B-Eng. **93**, 352-359 (2016).

[38] Z. Cao, X. Wang, J. Li, Y. Wu, H. Zhang, J. Guo, S. Wang, J. Alloy Compd. **696**, 498-502 (2017).

[39] J.M. Torralba, C.E. Costa, F. Velasco, J. Mater. Process. Tech. **133(1)**, 203-206 (2003).

[40] J.W. Kaczmar, K. Pietrzak, W. Wlosinski, J. Mater. Process. Tech. **106**, 58-67 (2000)

[41] C. Chen, Z. Ding, Q. Tan, H. Qi, Y. He, Powder Technol. **257**, 83-87 (2014).

[42] M. Rashad, F. Pan, Z. Yu, M. Asif H. Lin, R. Pan, Prog. Nat. Sci.-Mater. **25**, 460-470 (2015).